Remote Sensing Applications: Society and Environment 19 (2020) 100358

Contents lists available at ScienceDirect

Remote Sensing Applications: Society and Environment

journal homepage: http://www.elsevier.com/locate/rsase

A reasoned bibliography on SAR interferometry applications and outlook on big interferometric data processing

Muhagir El Kamali [a], Abdelgadir Abuelgasim [a,*], Ioannis Papoutsis [b], Constantinos Loupasakis [c], Charalampos Kontoes [b]

[a] National Water Center, Department of Geography and Urban Sustainability, United Arab Emirates University, Al Ain, Abu Dhabi, 15551, United Arab Emirates
[b] Institute for Astronomy, Astrophysics, Space Applications & Remote Sensing, National Observatory of AthensVas, Pavlou & I. Metaxa, GR-15 236, Penteli, Greece
[c] The National Technical University of Athens, School of Mining and Metallurgical Engineering, Department of Geological Sciences, Laboratory of Engineering Geology and Hydrogeology, Zographou Campus, 157 80, Athens, Greece

ARTICLE INFO

Keywords:
Land surface deformations
Synthetic aperture radar
Interferometry
PSI
SBAS
StaMPS
Big data analysis
Machine learning

ABSTRACT

In the past few decades, Synthetic Aperture Radar Interferometry (InSAR) has proven to be a reliable tool for monitoring land surface deformations occurring naturally (landslides, earthquakes, and volcanoes) or due to some anthropogenic activities, such as extraction of underground materials (, e.g., groundwater, oil, and gas) with acceptable accuracy. The availability of SAR data from various satellites have significantly improved this technology further notably with collecting data from different radar frequencies (X-, C-, and L-band), different spatial resolutions, increased revisit times and diverse imaging geometry including both along ascending and descending orbits. This review provides a description about the InSAR state-of-the-art technology and how it has been effectively used for detecting surface deformations. The techniques of Persistent Scatterer Interferometry, Small Baseline Subset, Stanford Method for Persistent Scatterers, and Offset Tracking are discussed. The paper also discusses the strengths and weaknesses of the different InSAR techniques currently employed in detecting surface deformations, concerning the various types of land cover. It then highlights the optimal methodology and data needs for these different land cover types. This work finally dives into the emergence of new technologies for processing big Earth Observation data and discusses the prospects of using machine/deep learning algorithms powered by advanced cloud computing infrastructure to mine new information hidden within InSAR products and associated land-surface deformations.

1. Introduction

Synthetic Aperture Radar Interferometry (InSAR) has been playing an essential role in monitoring changes in Earth's surface. It relies on measuring the phase difference between two or more complex values SAR images acquired at different times and/or different orbital positions. Primarily, there are three interferometric distributions; across-track interferometry, along-track interferometry, and repeat-pass across-track interferometry (Pepe and Calò, 2017).

SAR data becomes more available and accessible than before with variously operated radar wavelengths; for instance, P-band (65 cm), L-band (23 cm), C-band (5 cm), and X-band (3 cm). SAR images acquired with different look angle geometries over the same period could allow retrieving complete 3D displacements (Hue et al., 2017), where different acquisition modes are available, as well. The main differences are in the way of scanning the Earth's surface like generating a narrow swath when using Stripmap mode, a wide swath from ScanSAR mode, or viewing the scene from multiple angles when using Spotlight mode.

Since SAR systems operate in side-looking geometry, the displacement value measured will be in the RADAR Line-Of-Sight (LOS) direction (Ng et al., 2015). Measurements value in LOS direction is composed of vertical, easting and northing components (3D Deformations). Decomposing these components require multiple angle SAR scenes, but still retrieving the deformations of the northing component is very difficult. This because most of the new SAR satellites operate at near-polar orbits (parallel to N–S direction), so the viewing geometries are blind to N–S displacements. Retrieving 3D deformations have been investigated in many studies (Raucoules et al., 2013b; Darvishi et al., 2018) and it will be discussed later in section 2.

The main limitations for InSAR techniques are spatial and temporal

* Corresponding author.
E-mail address: a.abuelgasim@uaeu.ac.ae (A. Abuelgasim).

https://doi.org/10.1016/j.rsase.2020.100358
Received 28 October 2019; Received in revised form 29 June 2020; Accepted 30 June 2020
Available online 3 July 2020

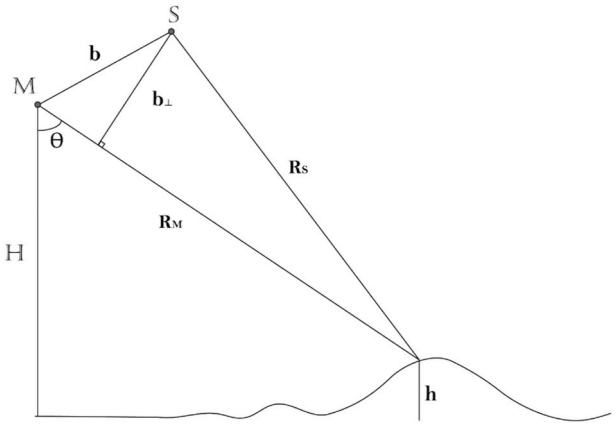

Fig. 1. Shows the InSAR geometry, where (M) is the location of first SAR acquisition, S is the location of second SAR acquisition, (b) is the spatial baseline, ($b_\perp$) is the perpendicular baseline, (θ) is the incident angle, (h) is the elevation of the observed point, and (H) is the altitude of the satellite.

decorrelations, which occur due to the large gap between two acquisitions in time or space, respectively. Landcover plays an important rule in performing InSAR techniques. For instance, the InSAR technique depends on finding coherent (stable) pixels during the deformations time to measure surface displacement. Therefore, it is easy to find coherent pixels over urban or mountain areas, but there is an effect of high buildings and mountains on the Radar signal; however, it is hard to find coherent pixels over vegetated areas.

The InSAR relies on the phase differences between two SAR images acquired at different times or different positions (Fig. 1). If we assumed that φ_M, φ_S, r_M, r_S, λ are phase of the first SAR image, phase of the second SAR image, range distance from the first SAR orbit, range distance from the second SAR orbit, and operated wavelength, respectively, the phase and phase difference (interferogram) can be obtained from the following equations:

$$\varphi_M = \frac{4\pi}{\lambda} r_M \tag{1}$$

$$\varphi_S = \frac{4\pi}{\lambda} r_S \tag{2}$$

$$\Delta\varphi = \frac{4\pi}{\lambda}\Delta r \tag{3}$$

Furthermore, Differential interferograms are generated by subtracting synthetic interferograms from the original interferogram (Moreira et al., 2013). There are two main categories for time series InSAR algorithms; Persistent Scatterer (PS) methods, Small Baseline (SB) methods, and combined methods. There are two main algorithms for PS; the first modeling the deformation in the time domain Permanent Scatterer Interferometry (PSI) (Ferretti et al., 2001) and Delft approach (Kampes, 2005), while the second modeling the spatial correlation between interferograms like StaMPS (Hooper et al., 2007). PSI relies on performing time series analysis on stable coherent targets called Persistent or Permanent Scatterers Scatterers (Ferretti et al., 2001). Some targets maintain high coherency for a long time even when observed with different geometrical characteristics (Crosetto et al., 2015). On the other hand, Small Baseline techniques analyze distributed targets that may be affected by spatial and temporal decorrelations (Pepe et al., 2015). These techniques generate wrapped interferograms (2π cycles) that need to be converted to one complete cycle, this procedure called phase unwrapping (Ferretti et al., 2007) and it is the most challenging process in InSAR.

Until recently, generating automated procedures for surface deformations were considered to be challenging due to the differences in geomorphological, geological, and geographical settings (Casagli et al.,

Table 1
Shows the surface deformations studies applied over different landcover.

Study	Landcover	SAR Data	Method
Rucci et al. (2012)	Deserts	Sentinel-1 A/B C-band	PSI
Amighpey and Arabi (2016)		ENVISAT SAR C-band	InSAR
Chang et al. (2018)		TerraSAR-X-band	InSAR
Gonnuru and Kumar (2018)		TerraSAR-X-band	PSI
Strozzi et al. (2008)	Glaciers	JERS-1 L-band	Offset Tracking
Short et al. (2014)		RADARSAT-2 C-band	DInSAR
Singhroy et al. (2014)		RADARSAT-2 C-band COSMO SkyMed X-band	SBAS
Singhroy and Li (2015)		RADARSAT-2 C-band COSMO SkyMed X-band	SBAS
Euillades et al. (2016)		COSMO-SkyMed X-band	PO – SBAS
Eriksen et al. (2017)		TerraSAR-X-band	InSAR
Strozzi et al. (2018a)		Sentinel-1 C-band	InSAR
Papoutsis et al. (2013)	Mountains	ENVISAT C-band	StaMPS PSI & SBAS
Raucoules et al. (2013b)		TerraSAR-X-band	Offset Tracking
Arab-Sedze et al. (2014)		ALOS-1 L-band	InSAR
Sansosti et al. (2014)		ENVISAT C-band COMO-SkyMed X-band	SBAS
Zebker and Zheng (2016)		COMO-SkyMed X-band ALOS-1 L-band	DInSAR
Dwivedi et al. (2017)		ENVISAT C-band	StaMPS PSI
Gama et al. (2017)		TerraSAR-X-band	SBAS
Hue et al. (2017)		ALOS-1 L-band	DInSAR
Jo et al. (2017)		TerraSAR-X-band	DInSAR
Kimura (2017)		ALOS-2 L-band	DInSAR
Luca et al. (2017)		ENVISAT C-band (Level 0)	SBAS
Polcari et al. (2017)		COMO-SkyMed X-band Sentinel-1A C-band	DInSAR
Strozzi et al. (2017)		ENVISAT C-band	PSI
Baek et al. (2018)		ALOS-2 L-band	DInSAR
Zhao et al. (2018)		ENVISAT C-band & ALOS-1 L-band	II-RATE
Zheng et al. (2018)		ENVISAT C-band Sentinel-1A C-band	TCP InSAR
Tao et al. (2012)	Rural Areas	ALOS-1 L-band	QCT DInSAR
Raucoules et al. (2013a)		ENVISAT C-band ALOS-1 L-band	PSI
Zhang et al. (2014)		TerraSAR-X-band	PSI
Dong et al. (2018)		ALOS-1 L-band ENVISAT C-band	CSI (PSI & SBAS)
Strozzi et al. (2018a,b)		ERS-1/2 C-band ENVISAT C-band ALOS-1 L-band ALOS-2 L-band TerraSAR-X-band Sentinel-1A C-band	PSI
Wei and Sandwell (2010)	Vegetation	ERS-1/2 C-band ALOS-1 L-band	SBAS
Reeves et al. (2014)		ERS-1/2 C-band	SBAS
Ng et al. (2015)		ALOS L-band	SqueeSAR
Darvishi et al. (2018)		Sentinel-1A C-band	SBAS
Liosis et al. (2018)		ENVISAT C-band ALOS-1 L-band Sentinel-1A C-band	SBAS
Zhang and Zhao (2018)		TerraSAR-X-band COMO-SkyMed X-band Sentinel-1A C-band ALOS-2 L-band	DInSAR
Calò et al. (2014)	Urban Areas	ERS-1/2 C-band ENVISAT C-band	SBAS

(*continued on next page*)

Table 1 (*continued*)

Study	Landcover	SAR Data	Method
		COMO-SkyMed X-band	
Chaussard et al. (2014)		ALOS-1 L-band	SB
Qu et al. (2014)		ENVISAT C-band ALOS-1 L-band TerraSAR-X-band	SBAS
Calò et al. (2015)		TerraSAR-X-band	SBAS
Chet et al. (2015)		Ground-Based SAR Ku-band	InSAR
Costantini et al. (2015)		ERS-1/2 C-band ENVISAT C-band COMO-SkyMed X-band	PSI
Normand and Heggy (2015)		RADARSAT-2 C-band	SBAS
Qu et al. (2015)		ERS-1/2 C-band ENVISAT C-band ALOS-1 L-band	StaMPS (PSI & SBAS)
Bai et al. (2016)		TerraSAR-X-band	StaMPS PSI
Casagli et al. (2016)		ERS-1/2 C-band ENVISAT C-band TerraSAR-X-band RADARSAT-2 C-band	PSI
Pepe et al. (2015)		ENVISAT C-band	SBAS
Scifoni et al. (2016)		ERS-1/2 C-band ENVISAT C-band	SBAS
Tong and Schmidt (2016)		ALOS-1 L-band	SBAS
Svigkas et al. (2017)		ERS-1/2 C-band ENVISAT C-band	StaMPS (PSI & SBAS)
Yu et al. (2017)		COMO-SkyMed X-band Sentinel-1A C-band	SBAS
Aslan et al. (2018)		ERS-1/2 C-band ENVISAT C-band Sentinel-1A C-band	PSI
Castellazzi et al. (2018)		ALOS-1 L-band	InSAR
Horst et al. (2018)		Sentinel-1A C-band	PSI
Haghighi and Motagh (2019)		ENVISAT C-band ALOS-1 L-band TerraSAR-X-band Sentinel-1A C-band	SB

2016).This review aims to illustrate the appropriate data and methods to retrieve surface deformations time series for different land cover types with selected case studies. Finally, it contains a concise discussion of challenges and future trends, especially to what concerns the processing of big interferometric data with novel technologies introduced by the ICT sector.

2. InSAR surface deformations applied over different landcover types

Various research studies have been conducted to retrieve land surface deformations using InSAR technique. Table 1 lists these studies in six landcover types; desert, mountains, rural, vegetation, and urban areas. Also, Table 1 shows used data and performed technique.

2.1. Desert

Desert areas are characterised by similar targets that have less decorrelation to shorter radar wavelengths. Performing PSI on X-band or C-band to observe ground displacement over desert areas is very efficient because there is an excellent possibility to obtain high PS density. Gonnuru and Kumar (2018) and Chang et al. (2018) studied surface deformations over an oil field in desert areas using X-ban SAR data obtained from TerraSAR-X. The first study performed the PSInSAR technique to reveal a maximum subsidence rate of 7.2–10 mm, while the second study utilized a spatiotemporal variogram model with the InSAR technique and found subsidence of 4 cm. Both studies interpreted the subsidence caused due to oil and gas extraction.

Amighpey and Arabi (2016) correlated land subsidence to water level changes over Yazd-Ardakan desert, Iran by utilizing the InSAR technique on ten images from ENVISAT C-band. This study found subsidence along Yazd-Ardakan road, west to Ardakan city, and south of Yazd city. Moreover, it concluded that the three areas a high degree of water-level decline.

2.2. Glaciers

Glacier surfaces are displaying relative faster motion than other landscapes, so there is no significant difference between various radar frequencies for detecting glacier surface motion. Euillades et al. (2016) investigated glacier surface velocities time series over Viedma Glacier using X-band SAR data acquired from COSMOSky-Med. The generated results demonstrated the technique's capability to obtain ice displacement with a mean surface velocity of 800 m/yr. Short et al. (2014) and Strozzi et al. (2018a) investigated land surface deformations over permafrost areas. Both studied used C-band SAR data, but the first one used SAR data from RADARSAT-2 while the second one used Sentinel-1. Short et al. (2014) revealed vertical displacements from 1 to −12.5 cm with a strong correlation with geology and field electrical conductivity measurements. Strozzi et al. (2018a) recorded various surface deformations rates from landscape to another with a maximum of 10 cm. Also, it suggested in-situ measurements for future work to enhance surface deformations detected over the permafrost landscape.

Singhroy et al. (2014) and Singhroy and Li (2015) studied the surface deformations resulted from steam injected to the subsurface in the process of oil sands over Athabasca and Alberta respectively, Northern Canada. Both studies used RADARSAT-2 and COSMO SkyMed with SBAS algorithm, levelling, gravimeters, tiltmeters, inclinometers, and GPS. Both studies showed a strong correlation between the uplift rates over the horizontal injector wells and the rate of steam injection. Moreover, the reservoir thickness and surface deformations are not correlated. Strozzi et al. (2008) studied the motion of Arctic glaciers at Svalbard, Novaya Zemlya and Franz-Josef land using offset tracking on JERS-1 L-band SAR images. This technique resulted in a consistent estimated error. It concluded that the offset tracking technique is strong and accurate with L-band SAR images for glacier movement estimation. This study raised the expectation of PALSAR data from the Advanced Land Observation Satellite (ALOS).

2.3. Mountains

In order to detect surface deformations using the InSAR technique over mountainous terrain, all available SAR data is applicable according to the various studies found in the literature. Hue et al. (2017) and Jo et al. (2017) investigated the surface deformations over Kilauea volcano in Hawaii islands using L-band from ALOS and X-band TerraSAR-X SAR data, respectively. Hue et al. (2017) performed a joint model to estimate 3D surface displacement from InSAR LOS measurement. The maximum surface displacements observed was −16 cm toward the caldera with magma volume change by $-4.6 \times 106\ m^3$. On the other hand, Jo et al. (2017) integrated deformation measurements of InSAR and GPS, but the atmospheric contribution on X-band was high due to the high terrain. RMS for the measurement of the deformation was 3.26 ± 1.32 cm and 2.95 ± 0.77 cm from ascending and descending datasets, respectively.

Raucoules et al. (2013b) and Gama et al. (2017) used X-band SAR data from TerraSAR-X but with different techniques. Raucoules et al. (2013b) performed offset tracking over La Valette landslide, South French Alps. This study observed a 14 m/yr maximum horizontal displacement rate and 11 m/yr maximum vertical rate. While Gama et al. (2017) performed SBAS over Carajás open-pit iron mine in Brazil. The observed maximum surface deformation was 500 mm/yr with good

consistency with leveling measurements.

Kimura (2017) and Baek et al. (2018) used L-band SAR data from the ALOS-2 platform with the DInSAR technique due to the Kumamoto earthquake occurred in 2016. Kimura (2017) retrieved 3D surface displacements and compared them with GNSS measurements. 3D surface displacements were 70, 50, and 30 cm for eastward, northward and upward, respectively. The comparison between InSAR deformations and GNSS measurements showed strong agreement with eastward and upward components and less agreement with the northward component. Baek et al. (2018) compared between traditional DInSAR with offset based phase unwrapping. The maximum surface deformations observed was 2 m in horizontal and vertical directions.

Polcari et al. (2017) investigated the local effects of the Central Italy seismic sequence 2016–2017 by combining COSMO-SkyMed and Sentinel-1 using the traditional DInSAR. This study observed displacement few centimetres with acceptable accuracy. Sansosti et al. (2014) investigated how the improvement of SAR technology increased the accuracy of the ground deformations measurement by performing the SBAS technique with X-band from COSMO-SkyMed and C-band from ERS-1/2 and ENVISAT datasets over Campi Flegrei and Mountain Etna volcanic areas in Italy. The physical processes behind the deformation's patterns were determined from the analysis of X-band data. The SBAS analysis allowed to detect non-linear deformations associated with anthropogenic activities. Second generation SAR sensors allowed to capture ground information with a higher level of spatial detail, both in natural and urban areas. Moreover, the capability to detect and monitor the temporal evolution of intra-building displacements in urban areas.

Zheng et al. (2018), Dwivedi et al. (2017), and Papoutsis et al. (2013) used only C-band SAR data from a different satellite to perform InSAR analysis. The first one integrated InSAR measurement with GRACE data to analyze the surface deformations over Xuzhou coalfield, China. This study found that the main reasons for surface subsidence were underground mining. The second two studies utilized the StaMPS technique on ENVISAT data, Dwivedi et al. (2017) observed surface displacements of −20 to 25 mm/yr over Tehri, India. Whereas Papoutsis et al. (2013) retrieved surface displacements range from −10 to 150 mm/yr over Santorini island, Greece.

The combination of poly-interferogram rate and time-series estimator algorithm (Π-RATE) were applied on SAR data acquired over Linfen-Yuncheng Basin, China, and allowed to observe the surface displacement of the basin by (Zhao et al., 2018). Π-RATE employs a pixel-wise approach to calculate deformations rates at pixels that are coherent in different numbers of interferograms, thus ensuring that useful information about the magnitude and spatial extent of the deformations field can be retrieved.

Mountainous areas represent a magnificent landscape to observe high PS density but also mountains produce a scattering problem by redirecting the radar signal. Most studies used different radar wavelengths to detect surface displacement over mountainous areas, and there is no advantage of using a specific frequency over others.

2.4. Rural

Rural areas have some aspects from urban areas and others from desert areas. Raucoules et al. (2013a) investigated land subsidence over 0.3 km^3 by performing the PSI technique on C-band ENVISAT and L-band ALOS-1. The main finding is the boundary of the subsidence area with a maximum deformations rate of 9 cm/yr. Zhang et al. (2014) applied the same technique by using TerraSAR X-band over the Northern part of the Tianjin city of China. This study split the LOS deformations to main and periodic deformations with maximum subsidence rate and acceleration 110 mm/yr and 19 mm/yr^2, respectively.

Strozzi et al. (2018b) investigated the surface motions from satellite InSAR and their relationship with landslides movements in Peru at Carhuaz city by using PSI technique but with more SAR data than the previous studies. These displacement rates were classified according the speed of movements; 0–2 cm/a, 2–10 cm/a, >10 cm/a, and undefined movement.

Tao et al. (2012) performed the Quasi-Coherent Targets (QCTs) based on DInSAR analysis using L-band SAR data from ALOS-1 over suburban Tianjin, China. It observed land subsidence rate of 2 cm/yr. Dong et al. (2018) combined persistent scatterers with distributed scatterers into an approach called Coherent Scatterer InSAR (CSI). The comparison between CSI and traditional InSAR showed that; the CSI is five times more time-consuming; the CSI requires four times more storage space, the CSI density points are ten times more, and the use of CSI with L-band data provided high-quality points over vegetated areas. This new method is facing the challenge of Sentinel-1 new generation.

2.5. Vegetation

Vegetation land cover is the most complicated land cover for SAR interferometry analysis. Since InSAR relies on finding pixels remain coherent for an extended period during the time-series analysis, vegetation land cover represents a fast-changing scattering characteristic due to the phonological cycle. Here are some studies that attempted to retrieve surface deformations over vegetation land cover.

Wei and Sandwell (2010) combined SAR data from ERS C-band and ALOS L-band with MODIS NDVI to investigate surface deformations over vegetated areas in California. This study showed that when the NDVI is less than 0.3, the interferograms from both satellites have high coherence. The comparison between ALOS and ERS showed that ALOS interferograms showed higher coherence than ERS generally, but it was less over sandy surfaces.

Reeves et al. (2014) investigated the uncertainty of implementing SBAS analysis for processing InSAR data to estimate surface deformations over agricultural areas in San Luis Valley (SLV), Colorado. This study relied on calculating the coherence for each interferogram using Gaussian distribution, and then it used these coherence values to estimate the uncertainty in the interferometric phase. This study proposed a method that allowed to estimate the uncertainty on a pixel by pixel, before performing SBAS analysis.

Liosis et al. (2018) studied the ground subsidence in the rural areas of Al Wagan, UAE, an arid region at the edge of Al-Rub' al-Khali desert, with generally flat terrain also including some dunes. Farms and vegetated areas occupy lands of Al Wagan. This study used data from ENVISAT, ALOS, and Sentinel-1A. The cumulative subsidence showed that there is a significant vertical deformation during summer. A direct relationship between subsidence obtained from SAR and groundwater level fluctuation have been found in this study. The main problem was spatial and temporal decorrelation in the study area. It suggested future work to include accurate field measurements using GNSS to validate the SAR time-series deformations.

Ng et al. (2015) studied the land deformations in the Gippsland Basin, Victoria, Australia using SqueeSAR approach by combining Persistent Scatterers with Distributed Scatterers on L-band ALOS SAR data. It suggested that the basin is relatively stable with displacements rate between 10 to −10 mm/yr.

2.6. Urban areas

Most of the studies in the related literature on retrieving surface deformations over urban areas used more than one radar wavelength, as finding coherent pixels are more feasible over urban areas.

Generally, the availability and wide distribution of C-band SAR data directed most of the researchers to use this type of data to monitor surface deformations over urban areas, such as Normand and Heggy (2015) from RADARSAT-2, Pepe et al. (2015) from ENVISAT, Horst et al. (2018) from Sentinel-1, Scifoni et al. (2016) from ERS-1/2 and ENVISAT, and Aslan et al. (2018) from ERS-1/2, ENVISAT, and Sentinel-1. Normand and Heggy (2015) retrieved surface deformations rate of −2 mm/yr over Montreal, Canada, and Horst et al. (2018) retrieved 120

mm/yr surface deformations rate. Pepe et al. (2015) retrieved 3D surface displacements by using the SBAS with the Minimum Acceleration technique, while Scifoni et al. (2016) used the same technique and correlate it with the geology.

Aslan et al. (2018) and Calò et al. (2015) investigated land surface deformations over Istanbul city, Turkey. The first one performed the PSI technique with C-band from ERS-1/-2, ENVISAT, and Sentinel-1 while the second one performed SBAS with X-band from TerraSAR-X. Both studies observed land subsidence around 10 mm/yr. Another study used TerraSAR-X data by Bai et al. (2016) via the StaMPS approach to retrieve maximum land surface subsidence and uplift rate 67.3 and 17.5 mm/yr, respectively over Wuhan city, China.

Chaussard et al. (2014) and Castellazzi et al. (2018) utilized L-band SAR data obtained from ALOS to detect surface deformations over Mexico city. The first study retrieved a maximum surface subsidence rate of 30 cm/yr with the small baseline technique. While the second study improved GRACE resolution with InSAR deformation measurements and revealed new subsidence regions with a maximum subsidence rate of 20 cm/yr. Tong and Schmidt (2016) used the same radar frequency with the SBAS technique and observed a relationship between landslide and precipitation at Cascade Landslide in Washington.

The combination of C-band data with X-band data to retrieve the surface displacement received intensive studies (e.g., Calò et al., 2014; Casagli et al., 2016; Costantini et al., 2015; Yu et al., 2017). However, Calò et al. (2014) and Yu et al. (2017) used the SBAS technique while Casagli et al. (2016) and Costantini et al. (2015) used the PSI technique. Calò et al. (2014), Costantini et al. (2015), and Yu et al. (2017) proved that X-band retrieved surface deformations in areas C-band unable to retrieve. Moreover, these studies concluded that accuracy is better when using X-band than C-band.

Qu et al. (2015) utilized the StaMPS technique with the combination of C-band with L-band SAR data to retrieve land subsidence up to 53 mm/yr and land uplift up to 20 mm/yr around Houston-Galveston, Texas. This study mentioned that the main reason for the ground deformations is groundwater and hydrocarbon withdrawal.

Qu et al. (2014) studied the land subsidence in Xi'an city, China using a combination of X-band, C-band, and L-band by performing the SBAS technique. This analysis detected four large subsidence zones and observing ground fissures and faults. Haghighi and Motagh (2019) performed the same combination with the same technique to study the ground surface deformations over Tehran plain in Iran. This analysis identified three dominant subsidence features; the southwest of Tehran, near IKA international airport, and Varamin with a maximum subsidence rate of more than 25 cm/yr.

Chet et al. (2015) presented experimental results of the Ground-Based Synthetic Aperture RADAR (GBSAR) in surface deformations monitoring at Peninsular of Malaysia using Ku-band. GBSAR has proved significant in-ground deformations monitoring by the capability of applied over broad areas, avoid weather conditions, and high change detection capability (sub-millimeter). The experiment showed that the GBSAR is capable of detecting sub-centimeter changes with an error of 5 mm and could attain a significantly high coherence of more than 0.9 between interferometric image pairs.

3. Discussions

InSAR technique has been applied to obtain surface deformations due to different causes; volcanic activities, landslide, subsidence, and oil, gas, and groundwater extraction, etc. with acceptable accuracy. This paper discusses retrieving the surface deformations over different land cover types from which appropriate SAR data and method for each land cover. Choosing the method and the data depends on some characteristics of the landcover such as the probability of determining PSs or DSs which differ from one landcover to another, but generally, PSs have more probability over the human-made structure while DSs have higher potentiality over natural surfaces. Another factor that needs to be considered when choosing the data and method is the rate of the surface movement; different landcover have a different response rate to the deformations such as glacier surface has a higher rate than the desert surface. From another point of view, the causes of the deformations affect the deformations rate, surface deformations due to groundwater exploitation has low rate than surface deformations due to landslide or volcanic activities.

Along with these considerations, some challenges are arising when using the InSAR technique for detecting surface deformations. The main challenge facing this technique is the error correction due to the travel radar signal through the atmosphere (Casu et al., 2011; Gudmundsson et al., 2002). Particles composing the atmosphere delay the radar signal, especially the wet parts due to water vapour. Other effects of atmospheric particles are introducing turbulence in the interferograms known as Atmospheric Phase Screen (APS). Moreover, variations of pressure, temperature, and relative humidity causing 15–20 cm of deformations, which is more than the surface deformations of interest. There are two general groups to estimate and remove APS. The first one depends on the statistical characteristics of the atmospheric phase, which it is correlated in space and uncorrelated in time. This approach uses spatial and temporal filters to estimate and remove the atmospheric phase. The second relies on using auxiliary information to estimate and remove the atmospheric phase, which include weather models, multi-spectral observations, or GPS measurements which they are hard to synchronise with SAR data, this lack in time will result in inaccuracies (; Fattahi et al., 2017b; Jung et al., 2013b).

The second challenge to use the InSAR technique for detecting 3D surface deformations. The 3D composed of three components; east-west, north-south, and up-down which is necessary to obtain data along both ascending and descending orbits (Michel et al., 1999; Samsonov and d'Oreye, 2012). The major challenge of retrieving these components is the north-south movement (Wright et al., 2004; Strozzi et al., 2002). Studies retrieved these three components observed high RMS error for the north-south component compared to the other components (Jung et al., 2011; Fialko et al., 2001). The difficulty of measuring this component due to radar satellites operation in near-polar orbit (north-south movement) which is parallel to this component and makes the satellite blind to move in this direction even with right-left – looking system and ascending and descending imaging. The right direct solution for this challenge is launching radar satellites operate in an east-west direction and combine it is data with current operating radar satellites.

The development of the new advanced imaging mode, Interferometric Wide (IW) swath mode by implementing Terrain Observation by Progressive Scans (TOPS) enhances the spatial coverage and image quality. TOPS has the capability to switch the radar antenna beam between the three sub-swaths to achieve wide swath coverage (250 km with a spatial resolution of 5×20m) in comparison with ScanSAR mode. The result of illuminating all targets on the ground by the entire azimuth antenna pattern mitigates the inaccurate estimation of doppler centroid mean frequency and leads to a constant signal-to-noise ratio (Fattahi et al., 2017a; Jung et al., 2013a; Mastro et al., 2020).

The future trends of this technology are providing near real-time information about surface deformations. The possibility of this trend coming from the second generation of SAR satellites which they provide high spatial and temporal resolution allowed to provide near real-time information. For example, Sentinel-2 satellites provide a revisit period of 5 days from one satellite over the equator and 2–3 days from two satellites at mid-latitude. This high temporal resolution will help to study the stages of fast movements and short period deformations.

However, as shown in the previous sections of this review, ground deformation mapping using diverse Persistent Scatterer techniques tailored for the various land cover types, have nearly become a commodity. The future active field of research for SAR interferometry arises from Big Data era; we now have and expect to have even more SAR sensors available to process, while the wealth of knowledge in interferometric stacks remains hidden. Therefore the challenges for the next

day is to unlock this potential and reflect the needs to 1) perform fully automatic unified and land-cover agnostic interferometric processing to monitor large geographic areas, even at national scale, and if possible address the challenge for generation of a 3D deformation field as discussed previously, 2) develop alert systems that inform decision-makers for hotspot areas undergoing significant deformation, 3) detect changes in the deformation regimes over critical assets in the urban environment, 4) and combine satellite interferometry products with other open data sources, potentially with industrial data, to create new processing chains the produce new scientific and business value.

4. Satellite interferometry and big data processing

This work dives into the emergence of new technologies for finding faster, cost-effective ways to process big Earth Observation data at scale. The focus of this part of the review is on the processing of big interferometric synthetic aperture radar datasets, rather than on generic remote sensing assets. We explore emerging technologies under three axes: (i) the availability of cloud infrastructures and high-performance computing environments that allow efficient multi-temporal PSI processing, even at national scale, (ii) the organisation of interferometric datasets in advanced geospatial databases called Data Cubes, which allow enhanced management of long time-series of interferometric measurements, and (iii) the prospects of using machine/deep learning algorithms powered by advanced cloud computing infrastructure to either generate more robust radar interferometry products or mine new information hidden within InSAR products and associated land-surface deformations, extract new knowledge and develop novel value-adding processing chains.

4.1. Interferometric processing on the cloud

The new generation of Earth Observation satellites from the Sentinel missions generate vast amounts of data that are not easily integrated into processing chains outside the ground segments of space agencies. Very often, public and private institutions aiming at delivering end-user services based on Earth Observation data do not possess the computing power and storage capacity to profit from these new data flows.

The Helix Nebula Initiative[1] started as a Public-Private-Partnership (PPP) to evaluate the needs of European compute-intense scientific research organisations and their exploitation of a Cloud Computing Infrastructure. Through the Helix Nebula Science Cloud initiative, a partnership was established between leading IT providers and some of Europe's biggest research centres that deployed and tested the infrastructure. One of the critical Use Cases of the Helix Nebula initiative is the one led by the European Space Agency (ESA), forming the ESA SuperSites Exploitation Platform (SSEP) Flagship.

SSEP developments comprised an instance of an exploitation platform for radar imagery in the context of geo-hazards, for the sharing of SAR data and the exploitation of interferometry processing on those data focusing on earthquake and volcano research. A large amount of SAR data is accessible to science communities dealing with interferometry, landslide and change detection. The SSEP project brings together existing software components and EO data in a portal that allows geohazard scientists to apply their algorithms and tools to analyze the data. Instead of downloading the data and applying their tools, users are presented with a wide selection of tools that they can apply within the portal, using cloud and grid technologies to achieve high performance and efficient use of communications links.

The SSEP flagship use case enabled Helix Nebula to mature its federated Cloud architecture and ultimately allowed ESA to analyze the feasibility and benefits of cloud deployments and paved the way to the development of the Thematic Exploitation Platform (TEP) initiatives. The TEP's canonical scenarios have moved the processing to the data, rather than the data to the users, thereby enabling ultra-fast data access and processing. This idea is an evolution of the Agency's Grid Processing on Demand (G-POD) system, the SSEP, and the integration of scientific applications and services for the FP7 EC projects (e.g. GEOWOW, SenSyF) and the experience gained with integration and deployment APIs leveraged within the Helix Nebula initiative.

Since 2018 and in order to facilitate and standardise access to data, the European Commission has funded the deployment of five cloud-based platforms providing centralised access to Copernicus data and information, as well as to cloud processing tools (open source and/or on a pay-per-use basis). These platforms are known as the DIAS, or Data and Information Access Services (DIAS). DIAS's objective is to become breeding grounds for innovative applications or "algorithm factories" allowing users to discover, manipulate, process and download Copernicus data and information.

Considering the processing of interferometric stacks on the cloud, there have recently been some research activities to automate PSI and/or SBAS processing chains. De Luca et al. (2015) have developed G-POD, a web tool for the unsupervised retrieval of Earth's surface deformation velocities using an online Parallel Small Baseline Subset (P-SBAS) approach (Casu et al., 2014) tailored for ERS and Envisat datasets. The ESA funded G-POD is a generic GRID-based operational environment coupled with high-performance and sizeable computing resources managed by GRID technologies. The architecture of the platform includes over 200 Working Nodes and more than 70 TB of EO data online. There are links with data providers and satellite imagery repositories.

The evolution of G-POD, so that it accommodates Sentinel-1A&B datasets, has been recently published by Manunta et al. (2019). The CNR-IREA team has put into place a methodology to automatically process coregistered interferometric vast swath stacks using enhanced spectral diversity (Fattahi et al., 2017a). It makes use of both multicore and multimode programming techniques, and consists of an ad hoc designed distributed storage implementation (Manunta et al., 2019), aimed at providing scalable performances for massive amounts of data to be processed (Zinno et al., 2015, 2016, Zinno et al., 2017). The approach has been tested for the whole Italian territory consisting of 2740 Sentinel-1 slices, while the results have been validated by nearly 500 GPS stations scattered over Italy.

According to our knowledge, there are a few other research activities to perform national scale the mapping using PSI on the cloud, which has not been published yet. These include the InSAR Norway[2] project, managed and coordinated by the Geological Survey of Norway. The project has processed Sentinel-1 SAR data from both ascending and descending orbits to generate deformation rate histories for two lines of sight vectors, therefore, unmixing vertical and horizontal displacements. Besides, the National Observatory of Athens developed a similar application that aims at national scale deformation mapping in Greece. The observatory has developed implementations of the InSAR Scientific Computing Environment (ISCE) and StaMPS software for interferogram formation and PSI analysis respectively, to be executed in distributed cloud environments. Finally, there are two similar applications for mapping land motion over the United Kingdom since 2015, TRE ALTAMIRA and Geomatic Ventures Limited (GVL). TRE ALTAMIRA has processed more than 7000 satellite radar images to generate a nationwide database of displacement measurements, while GVL using its in-house advanced interferometric SAR (InSAR) analysis of over 2000 Sentinel-1 to generate a relative land motion map.[3]

4.2. Data cubes for SAR interferometry datasets

EO data cube is a relatively new term, which describes the

[1] https://www.helix-nebula.eu/.

[2] https://insar.ngu.no/.

[3] https://www.geomaticventures.com/uk-map.

organisation (or "cubing") of raster data into a database-like structure that enables the efficient Spatio-temporal querying and processing of satellite images (BDVA, 2017). EO data, having the 5Vs of big data (Velocity, Volume, Value, Variety, and Veracity), have an inherent challenge; how to optimise information extraction from these data cubes? The opportunity that is addressed by the data cube concept is the exploitation of past and daily satellite observations to learn from the past, identify trends hidden in the big EO data, extract new knowledge and potentially short-term forecast some environmental variables.

Some of the most successful representations of the EO data cube concept implementations are the Australian Geoscience Data Cube (AGDC,[4] Lewis et al., 2017), the EO Data Cube (EODC[5]), the Earth System Data Cube (ESDC[6]), the Swiss Data Cube (Giuliani et al., 2017), the Common Sensing Data Cube (CSDC), the Ghana Data Cube (Haarpaintner et al., 5 2018), Earth on Amazon Web Services (EAWS[7]), and Google Earth Engine (GEE[8]). In contrast to the "traditional" database structure, which cannot handle (either at all or not in scale) geospatial data, the AGDC, EODC and ESDC rely on open source geospatial relation databases (e.g. PostgreSQL/PostGIS and Rasdaman, as by Baumann et al., 2019) to implement the EO cube concept. Less scalable GEE adopts a different approach to implement the concept and EAWS, which use proprietary cloud software and infrastructure to process the data in a file system-based concept.

Currently, most known Data Cube implementations rely on optical imagery (Dhu et al., 2017; Baumann et al., 2018) and only a few of them offer access to SAR products. Currently, two Data Cubes implementations focus exclusively on the use of SAR imagery. These are the SAR-Enabled Australian Data Cube (Ticehurst et al., 2019) and the Swiss Data Cube (Truckenbrodt et al., 2019). Both of them rely on the Open Data Cube (ODC[9]) initiative (Killough, 2018), populated with SAR data following the CEOS Analysis Ready Data (ARD) specifications. ODC is an open-source geospatial data management and analysis software project which has at its core a set of Python libraries and PostgreSQL database to allow working with geospatial raster data.

The Swiss Data Cube, in particular, is based on a cloud computing platform hosting 35 years and several TB of radiometrically terrain corrected SAR gamma nought backscatter data over the entire county. The Australian Data Cube, on the other hand, has created a unique dataset based on satellite interferometry by-products. This consists of multi-temporal coherence layers, which can be used for land-cover change (Plank, 2014) and/or vegetation growth (Tamm et al., 2016) studies.

An excellent example, although still at a concept level, for exploiting Data Cubes for deformation monitoring using interferometric techniques is presented by Lazecky et al., 2016). In this approach, a special geo-database is designed to ingest, store and manage coregistered Sentinel-1 bursts directly. Burst stacks are then processed on demand for user-selected areas of interest, using PSI as implemented by STaMPS software. At a post-processing phase, a data mining approach is applied for detecting deformation outlier estimates (Bakon et al., 2017) and creating a more reliable ground velocity pattern.

4.3. Deep/machine learning for satellite interferometry

While research on artificial intelligence has experienced significant growth over the last decade and data science has nearly become a commodity in various industries, deep learning has been one of the fastest-growing trends in big data analysis and was deemed one of the ten breakthrough technologies of 2013. In-depth learning research has been extensively pushed by Internet companies, such as Google, Baidu, Microsoft, and Facebook, for several image analysis tasks, including image indexing, segmentation, and object detection. However, it is only very recently that deep learning technologies were introduced to the EO research community (Zhu et al., 2017) for data mining and information extraction from big satellite data.

According to Soenen (2019), the ever-broadening use of deep learning in remote sensing is due to two trends: 1) availability of cloud computing infrastructure and resources, including GPUs; 2) the development of easy to use machine learning libraries like Google's Tensorflow[10], AWS SageMaker,[11] sci-kit learn,[12] and other open-source frameworks; and 3) an expanding ecosystem of services for creating labelled training data (Scale,[13] Figure Eight[14]) as well as open-labelled datasets tailored for satellite imagery, like SpaceNet on AWS.[15]

Here, we discuss the use of deep learning on interferometric synthetic aperture radar data. This is a new field that has started to gain increased attention in the past twelve months, and we expect that the number of research projects will kick-off. There are currently two families of research works related to deep learning on InSAR; the first one focuses on the automatic detection of ground deformation for setting-up an alert mechanism. This is accomplished through the recognition of interferometric phase fringes associated with ground deformation and eliminating background noise and fringes. The second family of deep learning processing chains is motivated by the well-formulated, ill-posed problem of phase unwrapping on satellite interferometry and medical imaging.

4.3.1. Volcanic ground deformation detection

Anantrasirichai et al. (2018) were the first ones ever to use deep learning on SAR interferograms to detect deformation. In their pioneer work, they processed more than 30,000 short-term wrapped interferograms to automatically detect volcanic ground deformation at over 900 volcanic areas around the world. They pre-train the network using an older archive of interferograms for ESA's Envisat satellite. Since most of the interferograms do not contain any deformation and in order to balance the training sample classes through data augmentation, the authors increase the number of positive examples (i.e. interferograms containing volcanic deformation) through shifting, flipping, rotating and distorting the shape of positive examples. They then employ a transfer learning strategy for the AlexNet Pre-trained Convolutional Neural Network (CNN). The model identified 104 positive results contained concentric fringes around the volcano, and for which even experts were unable to determine from a single interferogram whether the fringes were caused by volcanic deformation or atmospheric artefacts. Overall, the Anantrasirichai et al. (2018) proof-of-concept study demonstrated the ability of CNNs to identify rapidly deforming systems that generate multiple fringes in wrapped interferograms, which for a 12-day C-band interferogram, this corresponds to a deformation rate of 1.8 m/year.

Valade et al. (2019), build upon the study of Anantrasirichai et al. (2018) and trained a CNN on synthetically generated interferograms. The main progress is that Valade et al. (2019) is better at augmenting the deformation samples to prevent overfitting. They produce synthetic training data, allowing the generation of an unlimited number of interferograms, and avoiding the time-consuming task of labelling interferograms where deformation is identified through photo-interpretation. Besides, Valade et al., 2019 outputs clean phase

[4] http://www.datacube.org.au/.
[5] http://eodatacube.eu/.
[6] http://earthsystemdatacube.net/.
[7] https://aws.amazon.com/earth/.
[8] https://earthengine.google.com/.
[9] https://www.opendatacube.org/.
[10] https://www.tensorflow.org/.
[11] https://aws.amazon.com/sagemaker/.
[12] https://scikit-learn.org/stable/.
[13] https://scale.com/.
[14] https://www.figure-eight.com/.
[15] https://spacenetchallenge.github.io/datasets/datasetHomePage.html.

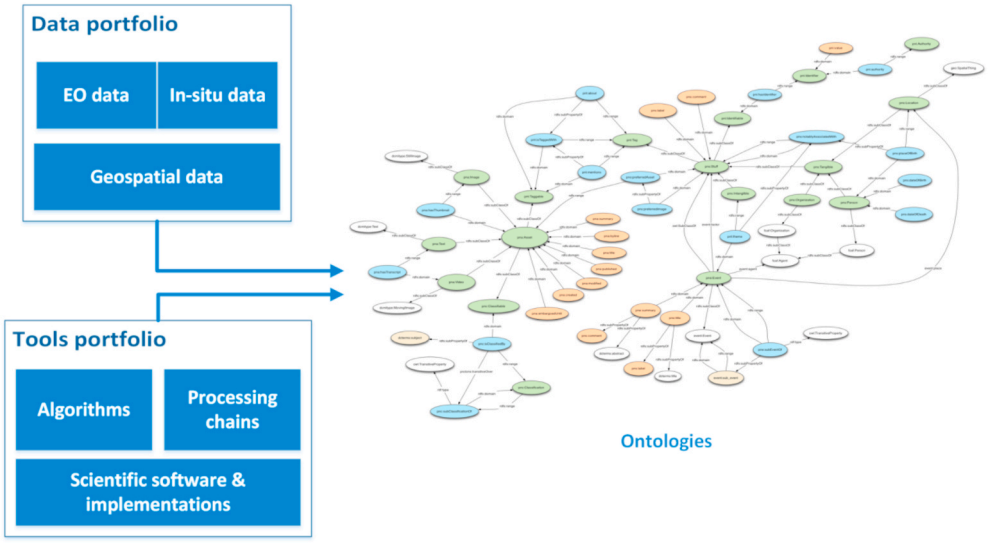

Fig. 2. Describing and linking space and processing assets using ontologies.

gradients which can be used directly to quantify volcanic deformation, whereas Anantrasirichai et al. (2018) estimate the probability a certain interferogram contain deformation fringes. Lastly, instead of using AlexNet as a pre-trained network, Valade et al. (2019) was designed from scratch and trained on a synthetic dataset, thereby allowing more flexibility.

Anantrasirichai and colleagues, however, in a new study by Anantrasirichai et al. (2019), also used synthetic interferograms to train the CNN model, however, based on analytic models simulating realistic deformation sources in volcanic settings. The synthetic interferograms in Anantrasirichai et al. (2019) are generated from i) synthetic deformation signals produced using simple elastic sources for earthquakes, dykes, sills and point pressure changes at magma chambers, ii) stratified atmospheric interferograms obtained from the Generic Atmospheric Correction Online Service (Yu et al., 2018), and iii) turbulent atmospheric interferograms simulated using the statistical characteristics of correlated noise in real interferograms (Biggs et al., 2007). This enhanced approach achieves better performance than Anantrasirichai et al. (2018) that uses real interferograms alone, decreasing the number of false positives by >80%.

The MATTCH project – Machine Learning methods for SAR-derived Time Series Trend Change Detection – has a similar objective to the research works presented above. MATTCH aims to apply Machine Learning techniques to InSAR data, for identifying persistent scatterers exhibiting displacement time series characterised by a change in trend or, more generally, an "anomalous behaviour". To capture the temporal dependencies in the long displacement time series, the leading Deep Learning architectures proposed by MATTCH for the analysis are Long Short-term Memory (LSTM) and Gate Recurrent Unit (GRU).

4.3.2. Phase unwrapping

Phase unwrapping is a classing signal processing problem that refers to recovering the original phase value (integer ambiguities) from its wrapped, modulo 2π form. Two-dimensional phase unwrapping problem arises in many applications such as optical measurement techniques (e.g., digital holographic interferometry and fringe projection profilometry, InSAR and Magnetic Resonance Imaging (MRI).

Feng et al., 2019 is one of the first works to train deep neural networks to perform fringe analysis, for a fringe projection profilometry use case. Spoorthi et al., 2018 propose a new framework for unwrapping the interferometric phase, formulating a semantic segmentation problem and using deep Fully Convolutional Neural Networks (FCN). Their model, termed as PhaseN consists of an encoder network, a corresponding decoder network followed by a pixel-wise classification layer. Training is performed using simulated data of wrapped and the corresponding unwrapped interferograms. This model achieves excellent performance under severe noise conditions and is computationally fast. Zhang et al., 2019, also formulate a semantic segmentation and propose a similar deep CNN, named DeepLabV3+, the problem for phase unwrapping. Zhang et al., 2019 performed benchmarks and showed that their deep learning model outperforms the conventional path-dependent and path-independent algorithms.

Given these latest advancements, there are new research projects that exploit computing depth and surface orientation maps directly from single images to derive an automated solution to unwrapping. Using deep networks with linked pipelines working at different spatial scales, the output maps are gradually refined, with information passing down from coarser to more beautiful scales. These research works have not yet published any results.

4.4. Semantic data mining

Sentinel-1 data for interferometric analysis, on the other hand, have two distinct characteristics: 1) they are made available on a free and open basis and 2) they are big data: indicatively the data volume of one month of Sentinel-1A acquisitions accounts for the entire ERS & Envisat archive. Similarly, Copernicus data sources are variable ranging from raw Sentinel data to in-situ information and model outputs (e.g. CAMS) with different quality standards, and in some instances such as the Sentinel-4 mission, data will arrive at high velocity.

Pure availability and accessibility of the plain interferometric data is only a first step. The EO data gains value only once it is s analysed, correlated and enriched with other data sources, and turned into information and knowledge. The sheer volume of the interferometric data - both per time and aggregated over time poses data management and analysis challenges that exceed the capabilities of current data management and analysis solutions for EO data.

The next logical step is to describe the data, products, and tools tailored for satellite interferometry, to create in other words ontologies that link different types of resources together, for a specific application (Fig. 2). Koubarakis et al. (2016), argue on the use of the linked data paradigm for significant data discovery and integration, using optical remote sensing use cases.

Semantic representation of interferometric data could pave the way for the use of other technologies, such as data mining and semantic querying. These technologies enable semantic-based data mining.

Indicatively, using these technologies one could ask the virtual database and retrieve suitable satellite imagery to conduct time-series interferometry, in previously high earthquake hazard areas in Chile, which contain or are close to cities with more than 50,000 inhabitants. Semantics-based data mining can lead the way for employing analytics applications and discover patterns in the available interferometric data.

5. Conclusions

Synthetic Aperture Radar Interferometry has become one of the most valuable techniques for detecting surface deformations in the last past decades. InSAR techniques have been utilized to detect surface deformations over different types of land cover. This paper can be considered as a manual for choosing the appropriate SAR data and methodology for various land cover types. However, selecting SAR data for specific land cover depends mainly on the characteristics of the surface and how it is reacted with the radar signal while choosing the appropriate methods depending on the radar signal response from the targeted surface. Moreover, there are combinations of techniques to improve the accuracy of detecting the surface deformations, and these combinations are varying from land cover type to another depending on the accuracy level that can be provided from InSAR techniques over the targeted land cover. This concludes that it is hard to generate one automated model to retrieve surface deformations over various land cover types.

Furthermore, this paper discusses the current challenges are facing InSAR techniques for surface deformations with the possible future trends for this technology. According to our view, the future of SAR interferometry lays in four axes: 1) large scale interferometric processing, 2) InSAR data cubes for analytics, 3) deep learning applications for deformation detection and 4) semantic-based interferometric data mining.

Declaration of competing interest

The authors whose names are listed in the manuscript certify that they have no affiliations with or involvement in any organization or entity with any financial interest or non-financial interest in the subject matter or materials discussed in the manuscript titled:A reasoned bibliography on SAR interferometry applications and outlook on big interferometric data processing

Acknowledgement

This work was funded by the National Water Center of the United Arab Emirates University under grant number 31R155-Research Center-NWC -3-2017.

Appendix A. Supplementary data

Supplementary data to this article can be found online at https://doi.org/10.1016/j.rsase.2020.100358.

References

Amighpey, M., Arabi, S., 2016. Studying land subsidence in Yazd province, Iran, by integration of InSAR and levelling measurements. Remote Sens. Appl.: Soc. Environ. 4, 1–8.

Anantrasirichai, N., Biggs, J., Albino, F., Hill, P., Bull, D.R., 2018. Application of machine learning to classification of volcanic deformation in routinely generated InSAR data. J. Geophys. Res.: Solid Earth 123, 6592–6606.

Anantrasirichai, N., Biggs, J., Albino, F., Bull, D., 2019. A deep learning approach to detecting volcano deformation from satellite imagery using synthetic datasets. Remote Sens. Environ. 230.

Arab-Sedze, M., Heggy, E., Bretar, F., Berveiller, D., Jacquemoud, S., 2014. Quantification of L-band InSAR coherence over volcanic areas using LiDAR and in situ measurements. Remote Sens. Environ. 152, 202–216.

Aslan, G., Cakir, Z., Ergintav, S., Lasserre, C., Renard, F., 2018. Analysis of secular ground motions in Istanbul from a long-term InSAR time-series (1992-2017). Rem. Sens. 10 (3), 408–425.

Baek, W.-K., Jung, H.-S., Chae, S.-H., 2018. Feasibility of ALOS2 PALSAR2 offset-based phase unwrapping of SAR interferogram in large and complex surface deformations. IEEE Access 6, 45951–45960.

Bai, L., Jiang, L., Wang, C., Sun, Q., 2016. Spatiotemporal characterization of land subsidence and uplift (2009–2010) over Wuhan in Central China revealed by TerraSAR-X InSAR analysis. Rem. Sens. 8 (4), 350–363.

Bakon, M., Oliveira, I., Perissin, D., Sousa, J.J., Papco, J., June 2017. A data mining approach for multivariate outlier detection in postprocessing of multitemporal InSAR results. IEEE J. Select. Top. Appl. Earth Observ. Remote Sens. 10 (6), 2791–2798.

Baumann, P., Rossi, A.P., Bell, B., Clements, O., Evans, B., Hoenig, H., Hogan, P., Kakaletris, G., Koltsida, P., Mantovani, S., et al., 2018. Fostering cross-disciplinary earth science through datacube analytics. In: Mathieu, P.-P., Aubrecht, C. (Eds.), Earth Observation Open Science and Innovation. Springer International Publishing, Cham, Switzerland, pp. 91–119.

Baumann, P., Misev, D., Merticariu, V., Huu, B.P., 2019. Datacubes: towards space/time analysis-ready data. In: Döllner, J., Jobst, M., Schmitz, P. (Eds.), Service-Oriented Mapping. Lecture Notes in Geoinformation and Cartography. Springer, Cham.

Biggs, J., Wright, T., Lu, Z., Parsons, B., 2007. Multi-interferogram method for measuring interseismic deformation: denali Fault, Alaska. Geophys. J. Int. 170 (3), 1165–1179.

Calò, F., Ardizzone, F., Castaldo, R., Lollino, P., Tizzani, P., Guzzetti, F., Lanari, R., Angeli, M.-G., Pontoni, F., Manunta, M., 2014. Enhanced landslide investigations through advanced DInSAR techniques: the Ivancich case study, Assisi, Italy. Remote Sens. Environ. 142, 69–82.

Calò, F., Abdikan, S., Görüm, T., Pepe, A., Kiliç, H., Şanli, F.B., 2015. The space-borne SBAS-DInSAR technique as a supporting tool for sustainable urban policies: the case of Istanbul megacity, Turkey. Rem. Sens. 7, 16519–16536.

Casagli, N., Cigna, F., Bianchini, S., Hölbling, D., Füreder, P., Righini, G., Del Conte, S., Friedl, B., Schneiderbauer, S., Iasio, C., Vlcko, J., Greif, V., Proske, H., Granica, K., Falco, S., Lozzi, S., Mora, O., Arnaud, A., Novali, F., Bianchi, M., 2016. Landslide mapping and monitoring by using radar and optical remote sensing: examples from the EC-FP7 project SAFER. Remote Sens. Appl.: Soc. Environ. 4, 92–108.

Castellazzi, P., Longuevergne, L., Martel, R., Rivera, A., Brouard, C., Chaussard, E., 2018. Quantitative mapping of groundwater depletion at the water management scale using a combined GRACE/InSAR approach. Remote Sens. Environ. 205, 408–418.

Casu, F., Manconi, A., Pepe, A., Lanari, R., 2011. Deformation time-series generation in areas characterized by large displacement dynamics: the SAR amplitude pixel-O_set SBAS technique. IEEE Trans. Geosci. Rem. Sens. 49, 2752–2763.

Casu, F., Elefante, S., Imperatore, P., Zinno, I., Manunta, M., De Luca, C., Lanari, R., 2014. SBAS-DInSAR parallel processing for deformation time-series computation. IEEE J. Sel. Top. Appl. Earth Obs. Remote Sens. 7, 3285–3296.

Chang, L., Ku, O., Hanssen, R.F., 2018. Identification of deformations pattern changes caused by enhanced oil recovery (EOR) using InSAR. Int. J. Rem. Sens. 1–11.

Chaussard, E., Wdowinski, S., Cabral-Cano, E., Amelung, F., 2014. Land subsidence in central Mexico detected by ALOS InSAR time-series. Remote Sens. Environ. 140, 94–106.

Chet, K.V., Siong, L.C., Hsin, W.H.H., Wei, L.L., Guey, C.W., Yam, C.M., Sze, L.T., Kit, C. Y., 2015. Ku-band ground-based SAR experiments for surface deformations monitoring. In: IEEE 5th Asia-Pacific Conference on Synthetic Aperture Radar (APSAR. IEEE, Singapore, pp. 641–644.

Costantini, M., Minati, F., Ciminelli, M.G., Ferretti, A., Costabile, S., 2015. Nationwide ground deformations monitoring by persistent scatterer interferometry. IEEE Int. Geosci. Remote Sens. Symp. (IGARSS) 1472–1475.

Crosetto, M., Monserrat, O., Cuevas-González, M., Devanthéry, N., Crippa, B., 2015. Persistent scatterer interferometry: a review. ISPRS J. Photogrammetry Remote Sens. 115, 78–89.

Darvishi, M., Schlögel, R., Kofler, C., Cuozzo, G., Rutzinger, M., Zieher, T., Toschi, I., Remondino, F., Mejia-Aguilar, A., Thiebes, B., Bruzzone, L., 2018. Sentinel-1 and ground-based sensors for continuous monitoring of the corvara landslide (south tyrol, Italy). Rem. Sens. 10 (11).

De Luca, C., Cuccu, R., Elefante, S., Zinno, I., Manunta, M., Casola, V., Rivolta, G., Lanari, R., Casu, F., 2015. An on-demand web tool for the unsupervised retrieval of Earth's surface deformation from SAR data: the P-SBAS service within the ESA G-POD environment. Rem. Sens. 7, 15630–15650.

Dhu, T., Dunn, B., Lewis, B., Lymburner, L., Mueller, N., Telfer, E., Lewis, A., McIntyre, A., Minchin, S., Phillips, C., 2017. Digital earth Australia – unlocking new value from earth observation data. Big Earth Data 1, 64–74.

Dong, J., Zhang, L., Tang, M., Liao, M., Xu, Q., Gong, J., Ao, M., 2018. Mapping landslide surface displacements with time-series SAR interferometry by combining persistent and distributed scatterers: a case study of Jiaju landslide in Danba, China. Remote Sens. Environ. 205, 180–198.

Dwivedi, R., Narayan, A.B., Tiwari, A., Singh, A.K., Dikshit, O., 2017. Optimal estimation of interferometric phase for measuring surface deformations. Int. J. Rem. Sens. 38 (5), 1339–1349.

Eriksen, H.Ø., Lauknes, T.R., Larsen, Y., Corner, G.D., Bergh, S.G., Dehls, J., Kierulf, H.P., 2017. Visualizing and interpreting surface displacement patterns on unstable slopes using multi-geometry satellite SAR interferometry (2D InSAR). Remote Sens. Environ. 191, 297–312.

Euillades, L.D., Euillades, P.A., Riveros, N.C., Masiokas, M.H., Ruiz, L., Pitte, P., Elefante, S., Casu, F., Balbarani, S., 2016. Detection of glaciers displacement time-series using SAR. Remote Sens. Environ. 184, 188–198.

Fattahi, H., Agram, P., Simons, M., 2017a. A network-based enhanced spectral diversity approach for TOPS time-series analysis. IEEE Trans. Geosci. Rem. Sens. 55 (2), 777–786.
Fattahi, H., Simons, M., Agram, P., 2017b. InSAR time-series estimation of the ionospheric phase delay: AnExtension of the split range-spectrum technique. IEEE Trans. Geosci. Rem. Sens. 55, 5984–5996.
Feng, Shijie, Chen, Qian, Gu, Guohua, Tao, Tianyang, Zhang, Liang, Hu, Yan, Yin, Wei, Zuo, Chao, 2019. Fringe pattern analysis using deep learning. Adv. Photon. 1 (2).
Ferretti, A., Prati, C., Rocca, F., 2001. Permanent scatterers in SAR interferometry. IEEE Trans. Geosci. Rem. Sens. 39 (2), 8–20.
Ferretti, A., Monti-Guarnieri, A., Prati, C., Rocca, F., Massonet, D., 2007. InSAR principles - Guidelines for SAR interferometry processing and interpretation. ESA Training Manual 19.
Fialko, Y., Simons, M., Agnew, D., 2001. The complete (3-D) surface displacement field in the epicentral area ofthe 1999 MW7.1 Hector Mine Earthquake, California, from space geodetic observations. Geophys. Res. Lett. 28, 3063–3066.
Gama, F.F., Cantone, A., Mura, J.C., Pasquali, P., Paradella, W.R., Santos, A.R., Silva, G. G., 2017. Monitoring subsidence of open pit iron mines at Carajȧs Province based on SBAS interferometric technique using TerraSAR-X data. Remote Sens. Appl.: Soc. Environ. 8, 211–219.
Giuliani, G., Chatenoux, B., De Bono, A., Rodila, D., Richard, J.-P., Allenbach, K., Dao, H., Peduzzi, P., 2017. Building an earth observations data cube: lessons learned from the Swiss data cube on generating analysis ready data. Big Earth Data 1 (1–2), 100–117.
Gonnuru, P., Kumar, S., 2018. PsInSAR based land subsidence estimation of Burgan oil field using TerraSAR-X data. Remote Sens. Appl.: Soc. Environ. 9, 17–25.
Gudmundsson, S., Sigmundsson, F., Carstensen, J.M., 2002. Three-dimensional surface motion maps estimated from combined interferometric synthetic aperture radar and GPS data. J. Geophys. Res. Solid Earth 107. ETG 13-1–ETG 13-14.
Haarpaintner, J., Killough, B., Ofori-Ampofo, S., Boamah, E.O., 5 November 2018. Advanced sentinel-1 analysis ready data for the Ghana open data cube and environmental monitoring. In: Proceedings of the International Workshop on Retrieval of Bio- & Geo-Physical Parameters from SAR Data for Land Applications. Oberpfaenhofen, Germany.
Haghighi, M.H., Motagh, M., 2019. Ground surface response to continuous compaction of aquifer system in Tehran, Iran: results from a long-term multi-sensor InSAR analysis. Remote Sens. Environ. 221, 534–550.
Hooper, A., Segall, P., Zebker, H., 2007. Persistent scatterer interferometric synthetic aperture radar for crustal deformations analysis, with application to Volcán Alcedo, Galápagos. J. Geophys. Res.: Solid Earth 112 (B7).
Horst, T.v.d., Rutten, M.M., Giesen, N.C.v.d., Hanssen, R.F., 2018. Monitoring land subsidence in Yangon, Myanmar using Sentinel-1 persistent scatterer interferometry and assessment of driving mechanisms. Remote Sens. Environ. 217, 101–110.
Hue, J., Ding, X.L., Zhang, L., Sun, Q., Li, Z.W., Zhu, J., Lu, Z., 2017. Estimation of 3-D surface displacement based on InSAR and deformations modeling. IEEE Trans. Geosci. Rem. Sens. 55 (4), 2007–2016.
Jo, M.-J., Jung, H.-S., Won, J.-S., 2017. Measurement of precise three-dimensional volcanic deformations via TerraSAR-X synthetic aperture radar interferometry. Remote Sens. Environ. 192, 228–237.
Jung, H.S., Lu, Z., Won, J.S., Poland, M.P., Miklius, A., 2011. Mapping three-dimensional surface deformation by combining multiple-aperture interferometry and conventional interferometry: application to the june 2007 eruption of Kilauea volcano, Hawaii. Geosci. Rem. Sens. Lett. IEEE 8, 34–38.
Jung, H.-S., Lu, Z., Zhang, L., 2013a. Feasibility of along-track displacement measurement from sentinel-1 interferometric wide-swath mode. IEEE Trans. Geosci. Rem. Sens. 51, 573–578.
Jung, H.-S., Lee, D.-T., Lu, Z., Won, J.-S., 2013b. Ionospheric correction of SAR interferograms by multiple-aperture interferometry. IEEE Trans. Geosci. Rem. Sens. 51, 3191–3199.
Kimura, H., 2017. Three-dimensional surface deformations mapping from multi-directional SAR interferograms. In: IEEE International Geoscience and Remote Sensing Symposium (IGARSS. IEEE, Fort Worth, TX, pp. 1692–1695.
Kampes, B, 2006. Radar Interferometry: Persistent Scatterer Technique;. Springer: Dordrecht, The Netherlands 12.
Killough, B., 2018. Overview of the open data cube initiative. In: Proceedings of the IEEE International Geoscience and Remote Sensing Symposium, pp. 8629–8632. Valencia, Spain, 22–27 July.
Koubarakis, M., et al., Sept. 2016. Managing big, linked, and open earth-observation data: using the TELEIOS\/LEO software stack. IEEE Geosci. Remote Sens. Mag. 4 (3), 23–37.
Lazecky, Milan, Canaslan Comut, Fatma, Bakon, Matus, Qin, Yuxiao, Perissin, Daniele, Hatton, Emma, Spaans, Karsten, Pablo, J., Mendez, Gonzalez, Guimaraes, Pedro, de Sousa, Joaquim J.M., Kocich, David, Ustun, Aydin, 2016. Concept of an effective sentinel-1 satellite SAR interferometry system. Procedia Comput. Sci. 100, 14–18.
Lewis, A., Oliver, S., Lymburner, L., Evans, B., Wyborn, L., Mueller, N., Raevksi, G., Hooke, J., Woodcock, R., Sixsmith, J., et al., 2017. The australian geoscience data cube — foundations and lessons learned. Remote Sens. Environ. 202, 276–292.
Liosis, N., Marpu, P.R., Pavlopoulos, K., Ouarda, T.B.M.J., 2018. Ground subsidence monitoring with SAR interferometry techniques in the rural area of Al Wagan, UAE. Remote Sens. Environ. 216, 276–288.
Luca, C.D., Zinno, I., Manunta, M., Lanari, R., Casu, F., 2017. Large areas surface deformations analysis through a cloud computing P-SBAS approach for massive processing of DInSAR time series. Remote Sens. Environ. 202, 3–17.
Manunta, Michele, De Luca, Claudio, Zinno, Ivana, Casu, Francesco, Manzo, Mariarosaria, Bonano, Manuela, Fusco, Adele, Pepe, Antonio, Onorato, Giovanni, Berardino, Paolo, De Martino, Prospero, Lanari, Riccardo, 2019. The parallel SBAS approach for sentinel-1 interferometric wide swath deformation time-series generation: algorithm description and products quality assessment. IEEE Trans. Geosci. Rem. Sens. 57 (9), 6269–6281.
Mastro, P., Serio, C., Masiello, G., Pepe, A., 2020. The multiple aperture SAR interferometry (MAI) technique for the detection of large ground displacement dynamics: an overview. Rem. Sens. 12, 1189.
Michel, R., Avouac, J.-P., Taboury, J., 1999. Measuring ground displacements from SAR amplitude images: application to the Landers Earthquake. Geophys. Res. Lett. 26, 875–878.
Moreira, A., Prats-Iraola, P., Younis, M., Krieger, G., Hajnsek, I., Papathanassiou, K.P., 2013. A tutorial on synthetic aperture radar. IEEE Geosci. Remote Sens. Mag. 1, 6–43.
Ng, A.-H., Ge, L., Li, X., 2015. Assessments of land subsidence in the Gippsland Basin of Australia using ALOS PALSAR data. Remote Sens. Environ. 159, 86–101.
Normand, J.C.L., Heggy, E., 2015. InSAR assessment of surface deformations in urban coastal terrains associated with groundwater dynamics. IEEE Trans. Geosci. Rem. Sens. 53 (12), 6356–6371.
Papoutsis, I., Papanikolaou, X., Floyd, M., Ji, K.H., Kontoes, C., Paradissis, D., Zacharis, V., 2013. Mapping inflation at Santorini volcano, Greece, using GPS and InSAR. Geophys. Res. Lett. 40 (2), 267–272.
Pepe, A., Calò, F., 2017. A review of interferometric synthetic aperture RADAR (InSAR) multi-track approaches for the retrieval of Earth's surface displacements. Appl. Sci. 7 (12), 1264–1303.
Pepe, A., Yang, Y., Manzo, M., Lanari, R., 2015. Improved EMCF-SBAS processing chain based on advanced techniques for the noise-filtering and selection of small baseline multi-look DInSAR interferograms. IEEE Trans. Geosci. Rem. Sens. 53 (8), 4394–4417.
Plank, S., 2014. Rapid damage assessment by means of multi-temporal SAR—a comprehensive review and outlook to Sentinel-1. Rem. Sens. 6, 4870–4906.
Polcari, M., Montuori, A., Bignami, C., Moro, M., Stramondo, S., Tolomei, C., 2017. Using multi-band InSAR data for detecting local deformations phenomena induced by the 2016–2017 Central Italy seismic sequence. Remote Sens. Environ. 201, 234–242.
Qu, F., Zhang, Q., Lu, Z., Zhao, C., Yang, C., Zhang, J., 2014. Land subsidence and ground fissures in Xi'an, China 2005–2012 revealed by multi-band InSAR time-series analysis. Remote Sens. Environ. 155, 366–376.
Qu, F., Lu, Z., Zhang, Q., Bawden, G.W., Kim, J.W., Zhao, C., Qu, W., 2015. Mapping ground deformations over Houston-Galveston, Texas using multi-temporal InSAR. Remote Sens. Environ. 169, 290–306.
Raucoules, D., Cartannaz, C., Mathieu, F., Midot, D., 2013a. Combined use of space-borne SAR interferometric techniques and ground-based measurements on a 0.3km2 subsidence phenomenon. Remote Sens. Environ. 139, 331–339.
Raucoules, D., Michele, M.D., Malet, J., Ulrich, P., 2013b. Time-variable 3D ground displacements from high-resolution synthetic aperture radar (SAR). application to La Valette landslide (South French Alps). Remote Sens. Environ. 139, 198–204.
Reeves, J.A., Knight, R., Zebker, H.A., 2014. An analysis of the uncertainty in InSAR deformations measurements for groundwater applications in agricultural areas. IEEE J. Select. Top. Appl. Earth Observ. Remote Sens. 7 (7), 2992–3001.
Rucci, A., Ferretti, A., Monti Guarnieri, A., Rocca, F., 2012. Sentinel 1 SAR interferometry applications: the outlook for sub millimeter measurements. Remote Sens. Environ. 120, 156–163.
Samsonov, S., d'Oreye, N., 2012. Multidimensional time-series analysis of ground deformation from multiple InSAR data sets applied to Virunga Volcanic Province. Geophys. J. Int. 191, 1095–1108.
Sansosti, E., Berardino, P., Bonano, M., Calò, F., Castaldo, R., Casu, F., Manunta, M., Manzo, M., Pepe, A., Pepe, S., Solaro, G., Tizzani, P., Zeni, G., Lanari, R., 2014. How second-generation SAR systems are impacting the analysis of ground deformations. Int. J. Appl. Earth Obs. Geoinf. 28, 1–11.
Scifoni, S., Bonano, M., Marsella, M., Sonnessa, A., Tagliafierro, V., Manunta, M., Lanari, R., Ojha, C., Sciotti, M., 2016. On the joint exploitation of long-term DInSAR time series and geological information for the investigation of ground settlements in the town of Roma (Italy). Remote Sens. Environ. 182, 113–127.
Short, N., Leblanc, A.-M., Sladen, W., Oldenborger, G., Mathon-Dufour, V., Brisco, B., 2014. RADARSAT-2 D-InSAR for ground displacement in permafrost terrain, validation from Iqaluit Airport, Baffin Island, Canada. Remote Sens. Environ. 141, 40–51.
Singhroy, V., Li, J., 2015. InSAR deformations monitoring of the Canadian oil sands from RADARSAT 2 and COSMO SkyMed images. In: IEEE International Geoscience and Remote Sensing Symposium (IGARSS, pp. 1523–1526, 2015.
Singhroy, V., Li, J., Samsonov, S., Shen, L., Pearse, J., 2014. InSAR Monitoring of Surface Deformations Induced by Steam Injection in the Athabasca Oil Sands, Canada, 2014 IEEE Geoscience and Remote Sensing Symposium, pp. 4796–4799.
Soenen, S., 2019. Deep Learning and SAR Applications. A short overview of advancements and challenges in earth observation application. Towards Data Science. https://towardsdatascience.com/deep-learning-and-sar-applications-81ba1a319def.
Spoorthi, G.E., Gorthi, Subrahmanyam, Gorthi, Rama Krishna Sai Subrahmanyam, 2018. PhaseNet: a deep convolutional neural network for two-dimensional phase unwrapping. IEEE Signal Process. Lett. 26 (1), 54–58.
Strozzi, T., Luckman, A., Murray, T., Wegmuller, U., Werner, C.L., 2002. Glacier motion estimation using SAR_set-tracking procedures. IEEE Trans. Geosci. Rem. Sens. 40, 2384–2391.
Strozzi, T., Kouraev, A., Wiesmann, A., Wegmüller, U., Sharov, A., Werner, C., 2008. Estimation of Arctic glacier motion with satellite L-band SAR data. Remote Sens. Environ. 12 (3), 636–645.
Strozzi, T., Caduff, R., Wegmüller, U., Raetzo, H., Hauser, M., 2017. Widespread surface subsidence measured with satellite SAR interferometry in the Swiss alpine range

associated with the construction of the Gotthard Base Tunnel. Remote Sens. Environ. 190, 1–12.
Strozzi, T., Antonova, S., Günther, F., Mätzler, E., Vieira, G., Wegmüller, U., Westermann, S., Bartsch, A., 2018a. Sentinel-1 SAR interferometry for surface deformations monitoring in low-land permafrost areas. Rem. Sens. 10.
Strozzi, T., Klimeš, J., Frey, H., Caduff, R., Huggel, C., Wegmüller, U., Rapr, A.C., 2018b. Satellite SAR interferometry for the improved assessment of the state of activity of landslides: a case study from the Cordilleras of Peru. Remote Sens. Environ. 217, 111–125.
Svigkas, N., Papoutsis, I., Loupasakis, C., et al., 2017. Environ. Earth Sci. 76, 195. https://doi.org/10.1007/s12665-017-6517-9.
Tamm, T., Zalite, K., Voomansik, K., Talgre, L., 2016. Relating sentinel-1 interferometric coherence to mowing events on grasslands. Rem. Sens. 8, 802–820.
Tao, L., Zhang, H., Wang, C., Tang, Y., 2012. Ground deformations retrieval using quasi-coherent targets DInSAR, with application to suburban area of Tianjin, China. IEEE J. Select. Top. Appl. Earth Observ. Remote Sens. 5 (3), 867–873.
Ticehurst, C., Zhou, Z.-S., Lehmann, E., Yuan, F., Thankappan, M., Rosenqvist, A., Lewis, B., Paget, M., 2019. Building a SAR-enabled data cube capability in Australia using SAR analysis ready data. Data 4, 100.
Tong, X., Schmidt, D., 2016. Active movement of the Cascade landslide complex in Washington from a coherence-based InSAR time series method. Remote Sens. Environ. 186, 405–415.
Truckenbrodt, J., Freemantle, T., Williams, C., Jones, T., Small, D., Dubois, C., Thiel, C., Rossi, C., Syriou, A., Giuliani, G., 2019. Towards sentinel-1 SAR analysis-ready data: a best practices assessment on preparing backscatter data for the cube. Data 4, 93.
Valade, S., Ley, A., Massimetti, F., D'Hondt, O., Laiolo, M., Coppola, D., Loibl, D., Hellwich, O., Walter, T.R., 2019. Towards global volcano monitoring using multisensor sentinel missions and artificial intelligence: the MOUNTS monitoring system. Rem. Sens. 11, 1528.
Wei, M., Sandwell, D.T., 2010. Decorrelation of L-band and C-band interferometry over vegetated areas in California. IEEE Trans. Geosci. Rem. Sens. 48 (7), 2942–2952.
Wright, T.J., Parsons, B.E., Lu, Z., 2004. Toward mapping surface deformation in three dimensions using InSAR. Geophys. Res. Lett. 31.
Yu, L., Yang, T., Zhao, Q., Liu, M., Pepe, A., 2017. The 2015–2016 ground displacements of the shanghai coastal area inferred from a combined COSMO-SkyMed/sentinel-1 DInSAR analysis. Rem. Sens. 9 (11), 1194–1212.
Yu, C., Li, Z., Penna, N.T., 2018. Interferometric synthetic aperture radar atmospheric correction using a GPS-based iterative tropospheric decomposition model. Remote Sens. Environ. 204, 109–121.
Zebker, H.A., Zheng, Y., 2016. Robust and efficient InSAR deformations time series processing. IEEE Int. Geosci. Remote Sens. Symp. (IGARSS) 3198–3200.
Zhang, P., Zhao, Z., 2018. Evaluation of data applicability for D-INSAR in areas covered by abundant vegetation. In: International Archives of the Photogrammetry, Remote Sensing and Spatial Information Sciences - ISPRS Archives, pp. 2277–2281.
Zhang, R., Liu, G., Li, T., Huang, L., Yu, B., Chen, Q., Li, Z., 2014. An integrated model for extracting surface deformations components by PSI time series. Geosci. Rem. Sens. Lett. IEEE 11 (2), 544–548.
Zhang, Teng, Jiang, Shaowei, Zhao, Zixin, Dixit, Krishna, Zhou, Xiaofei, Jia, Hou, Zhang, Yongbing, Yan, Chenggang, 2019. Rapid and robust two-dimensional phase unwrapping via deep learning. Optic Express 27, 23173–23185.
Zhao, C., Liu, C., Zhang, Q., Lu, Z., Yang, C., 2018. Deformations of Linfen-Yuncheng Basin (China) and its mechanisms revealed by II-RATE InSAR technique. Remote Sens. Environ. 218, 221–230.
Zheng, M., Deng, K., Fan, H., Du, S., 2018. Monitoring and analysis of surface deformations in mining area based on InSAR and GRACE. Rem. Sens. 10 (9).
Zhu, X.X., et al., 2017. Deep learning in remote sensing: a comprehensive review and list of resources. IEEE Geosci. Remote Sens. Mag. 5 (4), 8–36.
Zinno, I., et al., Oct. 2015. A first assessment of the P-SBAS DInSAR algorithm performances within a cloud computing environment. IEEE J. Sel. Topics Appl. Earth Observ. Remote Sens. 8 (10), 4675–4686.
Zinno, I., et al., Jan. 2016. Cloud computing for Earth surface deformation analysis via spaceborne radar imaging: a case study. IEEE Trans. Cloud Comput. 4 (1), 104–118.
Zinno, I., Casu, F., Luca, C.D., Elefante, S., Lanari, R., Manunta, M., 2017. A cloud computing solution for the efficient implementation of the P-SBAS DInSAR approach. IEEE J. Sel. Topics Appl. Earth Observ. Remote Sens. 10 (3), 802–817. Mar.